Talanta 121 (2014) 256–262

Contents lists available at ScienceDirect

Talanta

journal homepage: www.elsevier.com/locate/talanta

Preparation and adsorption of bovine serum albumin-imprinted polyacrylamide hydrogel membrane grafted on non-woven polypropylene

Kongyin Zhao [a,b,*], Beibei Lin [a,b], Wenkui Cui [a,b], Lingzhi Feng [a,b], Tian Chen [a,b], Junfu Wei [a,**]

[a] State Key Laboratory of Hollow Fiber Membrane Materials and Processes, Tianjin Polytechnic University, Tianjin 300387, China
[b] School of Material Science and Engineering, Tianjin Polytechnic University, Tianjin 300387, China

ARTICLE INFO

Article history:
Received 22 October 2013
Received in revised form
3 January 2014
Accepted 6 January 2014
Available online 18 January 2014

Keywords:
Protein molecular imprinting
Polypropylene non-woven
Grafting
Polyacrylamide hydrogel
Membrane
Adsorption

ABSTRACT

Bovine serum albumin (BSA) imprinted polypropylene (PP) fiber-grafted polyacrylamide (PAM) hydrogel membrane (PP-g-PAM MIP) was prepared using non-woven PP fiber as matrix, BSA as template molecule, and acrylamide (AM) as functional monomer via UV radiation-reduced polymerization in an aqueous phase. SEM, FT-IR, DSC and TG were used to characterize the PP grafted PAM hydrogel. Influence factors on the adsorption capacity of PP-g-PAM MIP were investigated, such as monomer concentration, cross-linker concentration, template molecule amount and pH values in BSA solution. The adsorption and recognition properties of PP-g-PAM MIP were evaluated and the results showed that the PP-g-PAM MIP exhibited an obvious improvement in terms of adsorption capacity for BSA as compared with non-imprinted ones. PP-g-PAM MIPs could recognize the template protein using Lys, Ova, BHb, and Glo as control proteins, and the selectivity factor (β) was above 2.0. The imprinting efficiency of PP-g-PAM MIP tended to be stable after three cycles and maintained 76% of the initial value of the imprinting efficiency even after five repetitions, which was more excellent than that of PAM microsphere. The PP-g-PAM MIP is low cost and easy to be prepared, which would show its potential applications in the fields of extracting and testing required proteins from cells or particulate samples.

1. Introduction

Molecular imprinting is a promising and evolving technology to synthesize tailor-made materials by means of co-polymerizing functional monomers and cross-linkers in the presence of desired template molecules [1]. Upon removal of the template molecules, pits or cavities are memorized and created in the molecularly imprinted polymer (MIP) matrix to complement to the template molecules sterically and chemically [2]. Compared with natural antibodies, MIPs exhibite lower selectivity. However, they have more advantages, such as chemical stability, excellent heat resistance, organic solvent resistance, low cost, and ease of mass preparation. Since 2000, great progress has been achieved in the research on molecular imprinting. Potential applications in chromatographic separations, solid-phase extraction, enzyme-like catalysis, bio-sensors, drug delivery, and other areas have been identified [3–10]. To date, the imprinting of low-molecular weight compounds (e.g., pharmaceuticals, pesticides, amino acids and peptides, nucleotide bases, steroids, and sugars) has now been well established [11–14].

However, several challenges remain in bio-macromolecule imprinting, such as those involving proteins, DNAs, and even whole cells and viruses. Many inherent problems of bio-macromolecules hinder the advancement of their imprinting, such as large molecular size, structural complexity, environmental sensitivity, and flexible conformation [15]. Given these obstacles, the fabrication of bio-macromolecule MIPs in the applications of diagnostics, bio-sensors, and bio-separation is still carried out [16–19]. An increasing number of researchers have focused on alternative strategies to overcome the aforementioned barriers from different viewpoints. One strategy is based on the surface imprinting technique to prepare MIP matrices on the surface, where cavities and pits are exposed [20–23]. The cavities and pits of the polymer matrix are accessible to protein molecules. Another method involves the use of hydrogel with soft and macroporous structure to manufacture an artificial antibody [24–31], which helps diffuse and elute the template. Given that the preparation conditions are beneficial in maintaining the native protein conformation, either synthetic or natural hydrogel materials are often selected as the hydrogel matrix.

* Corresponding author at: State Key Laboratory of Hollow Fiber Membrane Materials and Processes, School of Material Science and Engineering, Tianjin 300387, China. Tel.: +86 2283955362; fax: +86 228395055.
** Corresponding author. Tel.: +86 2283955898.
E-mail addresses: zhaokongyin@tjpu.edu.cn (K. Zhao), jfwei@tjpu.edu.cn (J. Wei).

0039-9140/$ - see front matter © 2014 Elsevier B.V. All rights reserved.
http://dx.doi.org/10.1016/j.talanta.2014.01.010

Biocompatible polyacrylamide (PAM) hydrogel possesses soft and wet macroporous structure that can allow the diffusion of large proteins. PAM chains contain many amide functional groups capable of forming strong interactions with peptide bonds in the protein even in polar solvents [32]. Hjerten et al. synthesized protein-imprinted hydrogels with a low degree of cross-linking, which demonstrated highly selective recognition ability for template molecules. Guo et al. [33] prepared bovine hemoglobin-imprinted chitosan microspheres by trapping selective soft PAM gel in the pores of the cross-linked chitosan beads. Pang et al. [34] reported bovine serum albumin (BSA)-imprinted PAM gel beads via inverse-phase seed suspension polymerization using high-density cross-linked gel beads as the core and low-density cross-linked PAM gel as the imprinting shell. Lu et al. [35] fabricated BSA and lysozyme surface-imprinted magnetic gel microspheres using magnetic composite gel microspheres as seeds via inverse-phase seed suspension polymerization. Qin et al. [36] fabricated lysozyme imprinted polymer beads using chloromethylated polystyrene beads as supports via surface-initiated living radical polymerization in aqueous media.

In previous studies, almost all protein-imprinted PAM hydrogels are particles or microspheres, whose shapes are difficult to maintain during recycling in aqueous solution. Microsphere preparation often uses organic solvent as a dispersion medium, which inevitably causes protein denaturation. Film materials have more advantages than microspheres or granules in several applications, such as extraction of required proteins from cells or particulate samples. However, obtaining a thin film of PAM hydrogel is difficult. Materials with neat form, good thermal stability, and good mechanical strength can be obtained via surface-grafting imprinting technology on inorganic or organic carrier. In recent years, several studies have reported on small molecule imprinting fibrous materials [37], which exhibit good flexibility and mechanical strength.

This paper presents a simple method of preparing protein-imprinted PAM hydrogel membrane using non-woven polypropylene (PP) fiber as matrix, BSA as template molecule, acrylamide (AM) as functional monomer, and N,N′-methylenebisacrylamide (MBA) as cross-linker via UV radiation-reduced polymerization. Factors that influence the adsorption capacity of MIPs were investigated, such as monomer concentration, cross-linker concentration, template molecule amount, and pH values in BSA solution. The rebinding and recognition properties of the PP-grafted imprinting PAM hydrogel membrane were evaluated.

2. Experimental

2.1. Materials

Non-woven polypropylene (PP) fiber (22 g/m^2) were purchased from Xianghehuaxin Non-woven Co., Ltd (Langfang, China). Acrylamide (AM) and N,N′-methylenebisacrylamide (MBA) were purchased from Chemistry Reagent Factory of Tianjin (Tianjin, China). Ammonium persulfate (APS), glacial acetic acid (HAc) and sodium dodecyl sulfate (SDS) were obtained from the Institute of Tianjin Guangfu Fine Chemicals (Tianjin, China). Bovine serum albumin (BSA, M_W 67 kDa, p*I* 4.9), lysozyme (Lys, M_W 14.4 kDa, p*I* 11), ovalbumin (Ova, M_W 43 kDa, p*I* 4.7), bovine hemoglobin (BHb, M_W 64.0 kDa, p*I* 6.9) and bovine γ-globulin (Glo, M_W 43 KDa, p*I* 7.1) were purchased from Lanji of Shanghai Science and Technology Development Company (Shanghai, China). All other chemicals were of analytical grade and used as received.

2.2. Preparation of non-woven PP-grafted BSA-imprinted PAM

Non-woven PP fiber (640 mg) was immersed in 33.6 mL of deionized (DI) water containing BSA (45 mg), AM (6 g), APS (60 mg), and MBA (60 mg). This mixture was incubated for 1 h at room temperature to allow the pre-assembly between the template molecules and the functional monomers. The non-woven PP was then placed on the quartz glass sheet, purged with nitrogen for 8 min, and sealed. Subsequent grafting polymerization was conducted for 1 h with ultraviolet (UV) irradiation at room temperature to produce the polymer hydrogel. The non-woven PP-grafted hydrogel was then repeatedly rinsed to remove the unreacted monomer and cross-linker with distilled water, and then, the template was eluted with acetic acid solution (10%, v/v) containing SDS (10%, w/v) until no BSA in the supernatant was detected by measuring the ultraviolet absorbance at 280 nm. Ultimately, the non-woven PP-grafted hydrogel was extensively washed with deionized water to remove remnant SDS and acetic acid. The non-woven PP-grafted BSA-imprinted PAM was prepared and labeled as PP-g-PAM MIP. The non-woven PP-grafted non-imprinted PAM was also prepared, which corresponds to PP-g-PAM MIP but without the template and was labeled as PP-g-PAM NIP.

2.3. Characterization

Fourier transform infrared (FT-IR) spectra of PP, PAM and PP-g-PAM were recorded with an Avatar 360 instrument (Nicolet, Waltham, MA, USA). The morphologies of PP and PP-g-PAM MIP were observed using a scanning electron microscope (FESEM; S-4800, HITACHI, Japan). PP and PP-g-PAM were dried at 55 °C under vacuum to constant weight. DSC and TG measurements were carried out for these dry samples using a NETZSCH STA 409 PC/PG (NETZSCH, Germany) analyzer at a heating rate of 10 °C/min from 20 °C to 200 °C under continuous flow of dry nitrogen.

2.4. Grafting rate of PAM

PP-g-PAM was dried at 50–70 °C in vacuum for several hours to remove water, and the grafting rate G was calculated using the following equation:

$$G(\%) = \left[(W_1 - W_0)/W_0\right] \times 100\% \quad (1)$$

where W_0 and W_1 were defined as the weight of the fiber before and after the grafting process, respectively.

2.5. Adsorption experiments

Adsorption experiments were carried out using a batch-wise adsorption method [23,27,33]. Wet PP-g-PAM MIPs or NIPs (1.0 g) were placed in each glass bottle containing 10 mL of 1.36 mg/mL BSA solutions to evaluate the imprinting efficiency and dynamic adsorption or various concentrations (0–3.0 mg/mL) and to determine the adsorption isotherms. BSA concentrations were measured using a UV–vis spectrophotometer at specific time intervals. The equilibrium adsorption capacity Q_e (mg/g) of the protein on the polymers was determined according to the following formula:

$$Q_e = (C_0 - C_e)V/W \quad (2)$$

where Q_e (mg/mL) is the equilibrium absorption, C_0 (mg/mL) is the initial BSA concentration, C_e (mg/mL) is the final concentration of BSA at equilibrium, V (mL) is the volume of BSA solution, and W (g) is the weight of MIPs or NIPs. The imprinting efficiency (IE) of MIPs was defined as follows:

$$IE = Q_{MIP}/Q_{NIP} \quad (3)$$

where Q_{MIP} and Q_{NIP} are the Q_e of MIPs and the corresponding NIPs, respectively.

The dynamic adsorption capacity Q_t (mg/g) at time t was calculated according to the following equation:

$$Q_t = (C_0 - C_t)V/W \quad (4)$$

where C_t (mg/mL) is the BSA concentration in the supernatant at time t. The Q_t of BSA on NIPs was also investigated following the steps previously mentioned.

2.6. Recognition performance

The recognition performance of PP-g-PAM can be evaluated by the static distribution coefficient K_D, the separation factor α, and the relative separation factor β [26,30]. Wet PP-g-PAM MIPs or NIPs (1.0 g) were placed into each glass bottle containing 10 mL of 1.36 mg/mL different protein solutions for 24 h to evaluate the recognition performances.

$$K_D = C_P/C_S \quad (5)$$

where C_P (mg/mL) and C_S (mg/mL) are the concentrations of the template adsorbed on the hydrogel and in the solution, respectively.

$$\alpha = K_{D1}/K_{D2} \quad (6)$$

where K_{D1} and K_{D2} are the static distribution coefficients of the template and other competitive proteins, respectively.

To compare the differences of molecular recognition on MIPs and NIPs, the relative separation factors β was introduced and defined as follows:

$$\beta = \alpha_I/\alpha_N \quad (7)$$

where α_I and α_N are the separation factors of the template on MIPs and NIPs, respectively.

3. Results and discussion

3.1. Effect factors on the grafting rate of PP-g-PAM

3.1.1. Effect of the monomer concentration on the grafting rate

Various monomer concentrations were used to study the effects of monomer concentration on the grafting rate of PP-g-PAM. Fig. S1 shows that the grafting rate sharply increased and reached equilibrium when the monomer concentration was 20 wt.%. When the concentration of monomer was low, the chance of diffusion of monomers with free radicals onto the surface of PP matrix was small; therefore, the grafting rate was also small. Increasing the monomer concentration increases the possibility of collision between free radicals and monomers; thus, the grafting rate was increased [38].

3.1.2. Effect of cross-linker concentrations on the grafting rate

Fig. S2 shows the effect of cross-linker concentrations on the grafting rate. The monomer concentration was fixed at 15 wt.% of the overall solution in this experiment. As observed in Fig. S2, increasing the cross-linker concentration resulted in an initial increase and then a decrease in the grafting rate of PAM on PP. When the cross-linker concentration was 2 wt.%, the grafting rate reached a maximum value of 162.5%.

3.2. Characterizations of PP-g-PAM MIP

3.2.1. SEM

Fig. 1 shows the surface SEM of PP and PP-g-PAM MIP. Compared with the PP fiber, the diameter and surface of PP-g-PAM MIPs became thick and rough, respectively, which was due to the uneven graft polymerization. Fig. 1(c) shows the surface magnification SEM of PP-g-PAM MIP. The surface of PP-g-PAM MIP was coarse, but the imprinting pores were not observed because water evaporation led to the shrinkage of the pores in vacuum.

3.2.2. FT-IR spectra

Fig. S3 shows the FT-IR spectra of PP, PAM, and PP-g-PAM. The appearance of the new adsorption bands at 1652 and 3213 cm^{-1}, which were not present in the spectrum of the original PP fibers, was attributed to the bending vibration of N–H and the stretching vibration of N–H. The existence of N–H bond indicates that AM was successfully grafted onto the PP fibers by UV radiation.

As shown in Fig. S4, the DSC curves of both PP and PP-g-PAM showed sharp peaks around 167 °C which was due to thermal decomposition of the polymer. While in the case of PP-g-PAM, the corresponding endothermic peak was shift to 166.5 °C and the shape of the exothermic peak was different. It was probably caused by the grafted branches, which disrupted the regularity of the chain structure and increased the spaces between the chains. Besides, the DSC curves of PP-g-PAM showed new endothermic peak at 134.26 °C, which did not display in PP, confirming the grafting of acrylamide onto PP.

3.2.3. Thermogravimetric (TG) and differential thermogravimetric (DTG) analysis

The integral results from TG analysis and DTG of PP and PP-g-PAM are shown in Fig. S5. In this figure, PP underwent weight loss in a temperature range of 439.9–499.4 °C during which the weight loss percent was 98.13%. This weight loss is attributed to the degradation of PP. PP-g-PAM had four pyrolysis stages. The first thermal degradation process occurred in the temperature range of 64.3–105.2 °C, and the weight loss rate was 9.18%. The weight loss in the first stage was attributed to bound water evaporation. The second stage occurred from 246.2 °C to 262.4 °C, and the weight loss rate was 10.06%. This weight loss was attributed to the degradation of PAM coated on the PP surface. The thermal degradation of PAM occurred in three pyrolysis stages. In the temperature range of 262.4–457.2 °C, ammonia molecule was liberated for every two amide groups, which resulted in the formation of imide. The thermal degradation of PP matrix occurred in four pyrolysis stages from 457.2 °C to 499.3 °C, and the weight loss was 32.09% [39].

3.3. Influencing factors on the adsorption capacity and imprinting efficiency of MIP

3.3.1. Effect of monomer concentration

The effects of monomer concentration on the adsorption capacity and imprinting efficiency are shown in Fig. S6. As observed in this figure, the adsorption of BSA on MIPs was much higher than that of NIPs. When the monomer concentration was 15 wt.%, the adsorption of BSA on both PP-g-PAM MIPs and NIPs almost reached the maximum. For MIPs, when the monomer concentration was above 20 wt.%, the adsorption capacity began to decline, whereas for NIPs, the adsorption capacity maintained the equilibrium. The increase in monomer concentration resulted in the increase in adsorption capacity of BSA on MIPs, which was due to the increase in grafting rate that led to the creation of more imprinting cavities in the PAM matrix. When the monomer concentration was above 20%, the grafting rate was further improved with increasing monomer concentration. However, the adsorption of BSA on MIPs slightly decreased, which was attributed to the difficulty in the absolute removal of the templates from the PAM matrix.

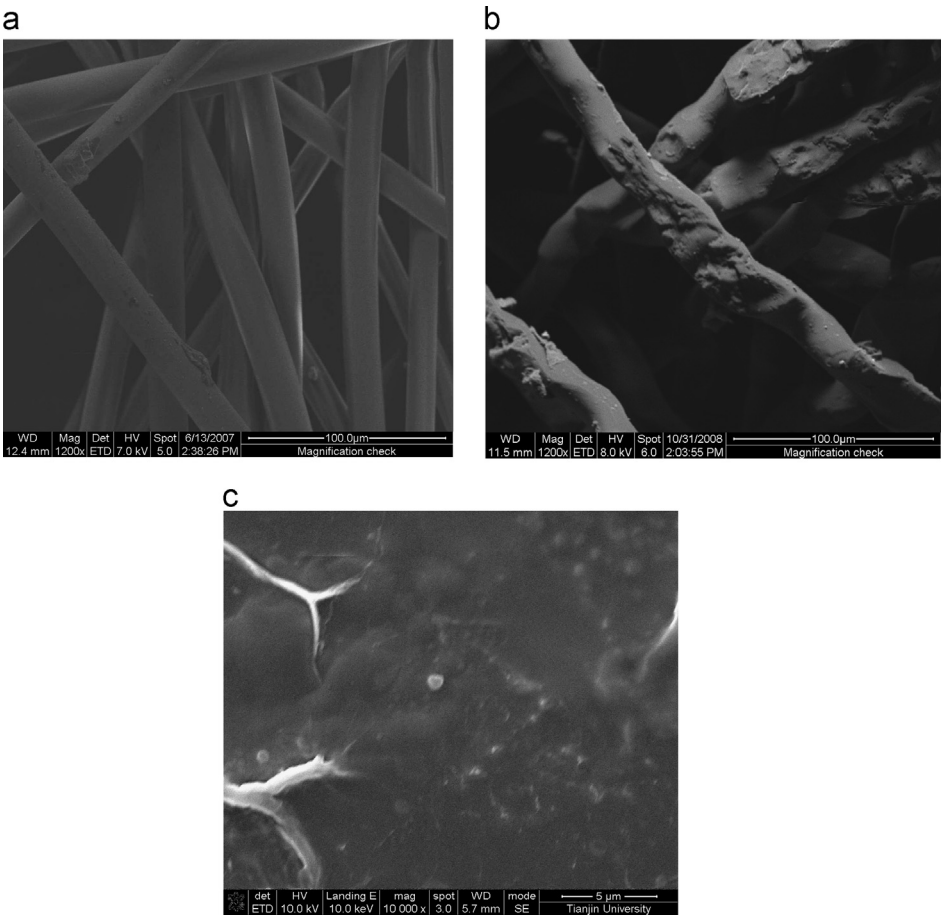

Fig. 1. Surface SEM of PP and PP-g-PAM MIP. (a) PP × 1200, (b) PP-g-PAM MIP × 1200, and (c) PP-g-PAM MIP × 10,000.

The maximum imprinting efficiency was 3.3 when the monomer concentration was 10 wt.%.

3.3.2. *Effect of cross-linker concentration*

The effects of different concentrations of cross-linker on the adsorption capacity and imprinting efficiency of PP-g-PAM MIP are shown in Fig. S7. When the concentration of cross-linker was 1 wt.%, the adsorption of BSA on MIPs reached the maximum and then decreased and ultimately reached equilibrium with increasing cross-linker concentration. When the concentration of the cross-linker was low, the adsorption capacity of BSA on MIPs was also low because the PAM hydrogel was too weak to remain in the imprinted cavities. When the concentration of cross-linker was above 1 wt.%, the adsorption capacity of BSA on MIPs declined with increasing cross-linker concentration. This result is due to excess cross-linked PAM hydrogel, which may hinder the diffusion of proteins.

3.3.3. *Effect of the amount of template molecule*

Given that the amount of cavities formed in PP-g-PAM gel depends on the template molecule content, different amounts of BSA were selected in the preparation of MIPs. Fig. S8 shows that the adsorption capacity increased with increasing template protein content. More BSA could produce more binding sites on the MIP surface, which resulted in the increase in adsorption capacity. However, the increase in adsorption capacity was not proportional to the BSA amount because part of the template proteins was deeply entrapped in the inner hydrogel and is difficult to remove. More BSA will be in the associated form with increasing BSA concentration, thereby making it more difficult to be imprinted. Increasing the amount of the template to obtain a large adsorption capacity is not an optimal choice.

3.3.4. *Effect of pH in BSA solution*

Fig. S9 shows the effect of pH value on the adsorption capacity and imprinting efficiency of PP-g-PAM MIPs. The adsorption capacity of BSA on MIPs was markedly higher than that of BSA on NIPs. When the pH values were in the range of 3.5–8.2, the maximum BSA adsorption on MIPs was achieved but then sharply decreased with increasing pH value. The adsorption capacity of BSA on NIPs was not notably changed in the range of pH values in the experiment. The imprinting efficiency reached the maximum when the pH was about 7 because the pH value affected the BSA conformation and charge. The pH values in the gel preparation process and rebinding conditions were close to 7.

3.4. *Adsorption kinetics of PP-g-PAM MIP and NIP*

Fig. 2 shows the adsorption dynamic curves of PP-g-PAM MIPs and NIPs. MIPs adsorbed more BSA than NIP. The equilibrium adsorption of BSA on MIPs was about three times as much as that of NIPs. For MIPs, the adsorption capacity initially increased in the first 50 min and the adsorption rate slowly increased as time went on. At an early time, a large number of imprinted cavities existed on the MIP surface so the template protein of BSA was accessible to the specific binding sites. Once the superficial imprinting sites were filled up, the adsorption rate significantly declined.

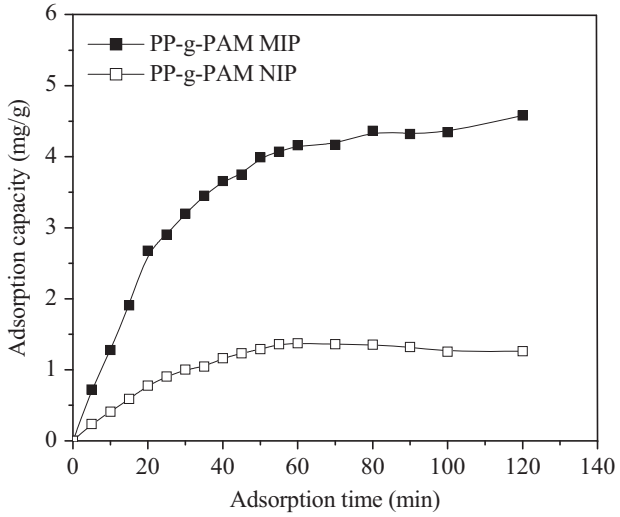

Fig. 2. Curve of adsorption kinetics.

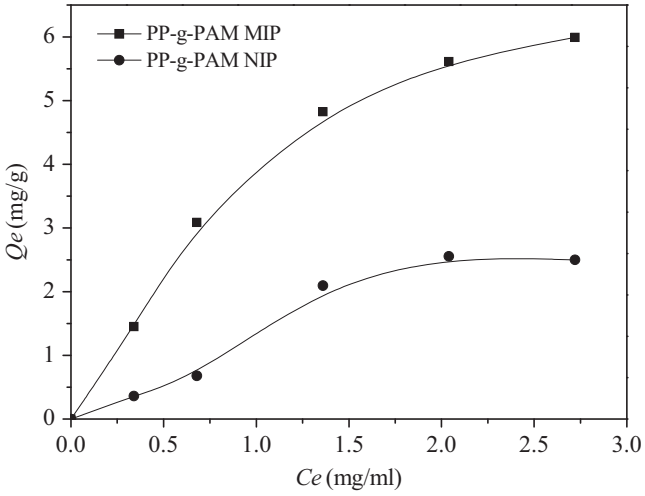

Fig. 3. Curve of adsorption thermodynamics of PP-g-PAM MIP and NIP.

The results in this rebinding process are in agreement with those in the common adsorption process [39].

3.5. Adsorption thermodynamics of PP-g-PAM MIP and NIP

The adsorption isotherm experiments for PP-g-PAM MIPs and NIPs were carried out using different BSA concentrations in the range of 0–3 mg/mL. At low BSA concentrations, the amount of BSA was not enough to fill up the specific binding pits and cavities (Fig. 3). However, almost all specific imprinted sites were gradually occupied and the adsorption capacity of MIPs became steady with increasing BSA concentration, and the saturation value was achieved at a BSA concentration of 3.0 mg/mL [40]. The maximum adsorption capacities of MIPs and NIPs were 5.99 and 2.50 mg/g, respectively. The results showed that MIPs had a higher adsorption capacity for BSA than that of NIPs. The binding curves of the polymer followed the Freundlich model equation:

$$Q_e = Q_f \cdot C_e^{1/n} \quad (8)$$

where C_e is the equilibrium concentration of BSA (mg/mL), Q_e (mg/g) is the adsorption capacity of BSA at the equilibrium concentration, Q_f is the rough adsorption capacity, and $1/n$ is the adsorption intensity. Fig. S10 shows the linearized plot of ln Q_e versus ln C_e for MIP and NIP. For both PP-g-PAM MIP and NIP, the ln Q_e versus ln C_e exhibited good linearity.

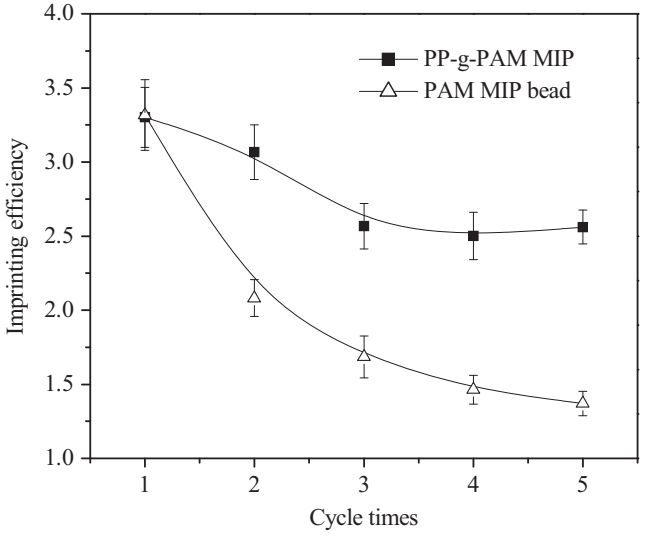

Fig. 4. Curves of regeneration properties of PP-g-PAM MIP.

3.6. Regeneration properties of PP-g-PAM MIP

Regeneration property is one of the most important advantages of MIPs, which has a great effect on their long-term application. The PP-g-PAM MIPs after BSA absorption were washed with 10% (v/v) acetic acid containing 10% (w/v) SDS to remove BSA and applied to rebind BSA. The regeneration property of BSA-imprinted PAM hydrogel bead was also based on a previous study [34]. Fig. 4 shows that the imprinting efficiency of PP-g-PAM MIPs gradually decreased with the cycle times (from 3.30 to 2.56) and reached a stable value after three cycle times. The imprinting efficiency of PP-g-PAM MIPs was maintained at 76% of the initial value even after five cycles. However, the imprinting efficiency of BSA-imprinted PAM microspheres continually declined with increasing cycle times. After five cycle times, the imprinting effect almost disappeared. This result is probably due to the soft texture of gel microspheres, which cannot stabilize the shape of the binding sites. By contrast, the strength of PP-g-PAM MIPs was significantly improved and the shape of the binding sites was almost stabilized.

3.7. Recognition performance of PP-g-PAM MIP

The selectivity test of PP-g-PAM MIP was carried out at equilibrium adsorption conditions using Lys, Ova, BHb, and Glo as competitive proteins. Fig. 5 shows the adsorption capacities of MIP and NIP for BSA and competitive proteins. The imprinting factor (α) and selectivity factor (β) of PP-g-PAM MIPs and NIPs are shown in Fig. 6. MIP exhibited good adsorption selectivity for the template BSA. The Q of BSA on MIPs was higher than that of Lys, Ova, BHb and Glo. In the binding process, many specific recognition sites with respect to template protein were generated on the MIP surface. Thus, the template protein was strongly bound to the polymers. For the competitive proteins, although Lys was small enough to diffuse into the imprinting cavities, the recognition sites were not complementary to Lys; thus, it had less chance to be adsorbed on the PP-g-PAM MIPs. The molecular volume of γ-Glo was larger than that of BSA, and the imprinting cavities were not complementary to it. The adsorption capacity of γ-Glo on MIPs was much lower than that of any protein used in the experiment. By comparison, NIPs adsorbed much less template than that of

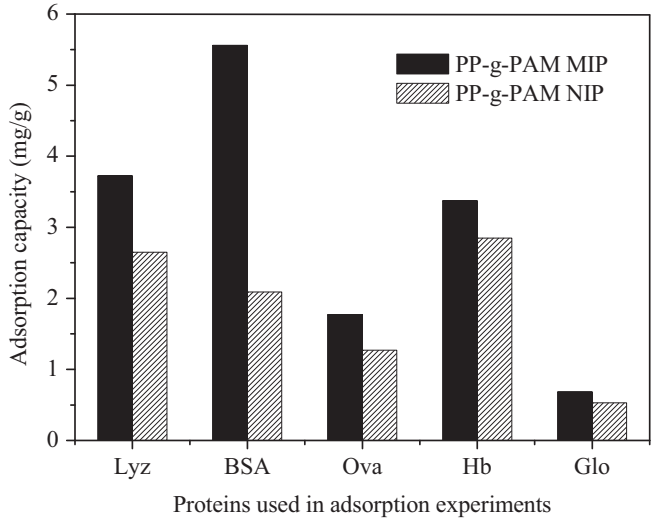

Fig. 5. Adsorption capacities of PP-g-PAM MIP and NIP with different proteins.

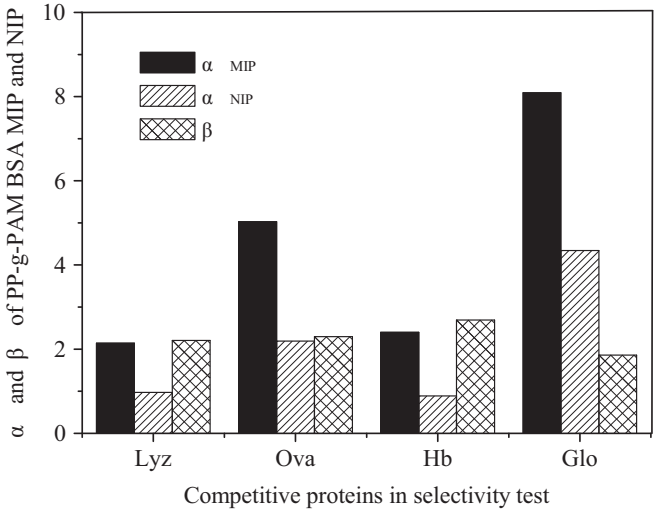

Fig. 6. Imprinting factor (α) and selectivity factor (β) of PP-g-PAM BSA MIP.

MIPs. This result is attributed to the failure of NIPs to form specific recognition sites because of the absence of template proteins.

This non-woven PP fiber-grafted hydrogel MIPs is low-cost and is easy to prepare and use. It has potential applications in the fields of extraction of required proteins from cells, cell culture, and controlled release of proteins. The extraction of required protein from mixed proteins in complicated samples is under investigation, and the results will be reported in another paper.

4. Conclusion

BSA-imprinted PP fiber-grafted PAM hydrogel membrane was successfully prepared using non-woven PP fiber as matrix, BSA as template molecule, and AM as functional monomer via UV radiation-reduced polymerization in an aqueous phase. SEM and FT-IR results indicated that PAM was grafted onto the non-woven PP fiber.

The results of adsorption dynamics and isotherms showed that PP-g-PAM MIPs exhibited an obvious improvement in adsorption capacity for BSA compared with that of non-imprinted PAM. PP-g-PAM MIPs could recognize the template protein using Lys, Ova, BHb, and Glo as control proteins, and the selectivity factor (β) was above 2.0. The imprinting efficiency of PP-g-PAM MIP tended to be stable after three cycles and maintained 76% of the initial value of the imprinting efficiency even after five repetitions, which was more excellent than that of PAM microsphere.

Acknowledgments

The research is supported by the National Natural Science Foundation of China (51103102), Ministry of education doctoral new teacher fund (20111201120004), Funds for technological innovation of small and medium enterprise in Tianjin (12ZXCXGX20700) and the Tianjin Colleges Science and Technology Development Fund (20100308).

Appendix A. Supplementary material

Supplementary data associated with this article can be found in the online version at http://dx.doi.org/10.1016/j.talanta.2014.01.010.

References

[1] Y. Lei, K. Masbach, Chem. Mater. 20 (2008) 859–868.
[2] K. Haupt, K. Mosbach, Chem. Rev. 100 (2000) 2495–2504.
[3] E. Verheyen, J.P. Schillemans, M. Wijk, M.A. Demeniex, W.E. Hennink, C.F. Nostrum, Biomaterials 32 (2011) 3008–3020.
[4] C. Yu, K. Mosbach, J. Chromatogr. A 888 (2000) 63–72.
[5] F.T.C. Moreira, R.A.F. Dutrab, J.P.C. Noronhad, A.L. Cunhae, M.G.F. Sales, A.L. Cunhae, M. Goreti, F. Sales, Biosens. Bioelectron. 28 (2011) 243–250.
[6] M.E. Byrne, K. Park, N.A. Peppas, Adv. Drug Deliv. Rev. 54 (2002) 149–161.
[7] J.Z. Hilt, M.E. Byrne, Adv. Drug Deliv. Rev. 56 (2004) 1599–1620.
[8] L. Han, Y. Shu, X. Wang, X.W. Chen, J.H. Wang, Anal. Bioanal. Chem. 405 (2013) 8799–8806.
[9] M. Hao, X.W. Chen, J.H. Wang, J. Mater. Chem. 21 (2011) 14857–14863.
[10] Z. Du, Y.L. Yu, X.W. Chen, J.H. Wang, Chem. Eur. J. 13 (2007) 9679–9685.
[11] Y.P. Huang, Z.S. Liu, C. Zheng, R.Y. Gao, Electrophoresis 30 (2009) 155–162.
[12] N. Bereli, Y. Saylan, L. Uzun, R. Say, A. Denizli, Sep. Purif. Technol. 82 (2011) 28–35.
[13] M. Abdouss, S. Azodi–Deilami, E. Asadi, Z. Shariatinia, J. Mater. Sci. M 23 (2012) 1543–1552.
[14] T. Shiomi, M. Matsui, F. Mizukami, K. Sakaguchi, Biomaterials 26 (2005) 5564–5571.
[15] H.Q. Shi, W.B. Tsai, M.D. Garrison, S. Ferrari, B.D. Ratner, Nature 398 (1999) 593–597.
[16] K.K. Tadi, R.V. Motghare, J. Mol. Model. 19 (2013) (3385–3339).
[17] Y.X. Li, Y.J. Li, M. Hong, Q. Bin, Z.Y. Lin, Z. Lin, Z.W. Cai, G.N. Chen, Biosens. Bioelectron. 42 (2013) 612–617.
[18] B.B. Prasad, A. Prasad, M.P. Tiwari, Talanta 109 (2013) 52–60.
[19] M.S. Zhang, J.R. Huang, P. Yu, X. Chen, Talanta 81 (2010) 162–166.
[20] K.Y. Zhao, G.X. Cheng, J.J. Huang, X.G. Ying, React. Funct. Polym. 68 (2008) 732–741.
[21] Y.T. Wang, Y.X. Zhou, J. Sokolov, B. Rigas, K. Levon, M. Rafailovich, Biosens. Bioelectron. 24 (2008) 162–166.
[22] W. Lei, Z.H. Meng, W.b. Zhang, L.Y. Zhang, M. Xue, W. Wang, Talanta 99 (2012) 966–971.
[23] T.Y. Guo, Y.Q. Xia, G.J. Hao, M.D. Song, B.H. Zhang, Biomaterials 25 (2004) 5905–5912.
[24] X.S. Pang, G.X. Cheng, Y.H. Zhang, S.L. Lu, React. Funct. Polym. 66 (2006) 1182–1188.
[25] D. Ran, Y.Z. Wang, X.P. Jia, C. Nie, Anal. Chim. Acta. 723 (2012) 45–53.
[26] L. Qin, X.W. He, W. Zhang, Anal. Chem. 81 (2009) 7206–7216.
[27] X.S. Pang, G.X. Cheng, S.L. Lu, E.J. Tang, Anal. Bioanal. Chem. 384 (2006) 225–230.
[28] G.Q. Fu, J.C. Zhao, H. Yu, L. Liu, B.L. He, React. Funct. Polym. 67 (2007) 442–450.
[29] G.Q. Fu, H.G. He, Z.H Chai, H.C. Chen, J. Kong, Y. Wang, Y.Z. Jiang, Anal. Chem. 83 (2011) 1431–1436.
[30] E.P. Herrero, E.M. DelValle, N.A. Peppas, Ind. Eng. Chem. Res. 49 (2010) 9811–9814.
[31] C. Yu, K. Mosbach, J. Org. Chem. 62 (1997) 4057–4064.
[32] T.Y. Guo, Y.Q. Xia, J. Wang, M.D. Song, B.H. Zhang, Biomaterials 26 (2005) 5737–5745.
[33] X.S. Pang, G.X. Cheng, R.S. Li, S.L. Lu, Y.H. Zhang, Anal. Chim. Acta 550 (2005) 13–17.
[34] S.L. Lu, G.X. Cheng, X.S. Pang, J. Appl. Polym. Sci. 99 (2006) 2401–2407.

[35] L. Qin, X.W. He, W. Zhang, W.Y. Li, Y.K. Zhang, J. Chromatogr. A 1216 (2009) 807–814.
[36] H. Tokuyama, S. Naohara, M. Fujioka, S. Sakohara, React. Funct. Polym. 68 (2008) 182–188.
[37] A.H.M. Yusof, M. Ulbricht, J. Membr. Sci. 311 (2008) 294–305.
[38] H.D. Burrows, H.A. Ellis, S.I. Utah, Polymer 22 (1981) 1740–1744.
[39] C.J. Tan, Y.W. Tong, Anal. Chem. 79 (2007) 299–306.
[40] F. Bonini, S. Piletsky, A.P.F. Turner, A. Speghini, A. Bossi, Biosens. Bioelectron. 22 (2007) 2322–2328.